THE EQUIVALENT CIRCUIT AND THE TEMPERATURE DEPENDENCE OF DUAL-MODE RING-RESONATORS

GAMAL ABEDEL-RAHIEM* and L. JACHIMOVITS
Department of Microwave Telecommunication,
Technical University, H-1521 Budapest

Received Jan. 2, 1984

Presented by Prof. Dr. I. Bozsóki

Summary

In this paper, the equivalent circuit of the dual mode ring resonators is derived which is in good agreement with the experimental results. The temperature dependence of the ring resonator resonance frequency is discussed.

Introduction

Ring resonators are used as resonators, antennas and other circuit elements for microwave integrated circuits, e.g. in circulators, hybrid junctions, filters, and directional filters. A ring resonator exhibits filtering properties, depending on the arrangement of the coupling lines [1]. Ring resonator resonance frequencies can be determined by using the H-wall-model theory [2]. The resonant modes are TM_{mno}, and the eigenvalues can be determined from [2]:

$$J'_m(K_{mn}a)N'_m(K_{mn}b)-J'(K_{mn}b)N'_m(K_{mn}a)=0 \tag{1}$$

where a, and b are the inner and outer radii of the ring resonator, $J_m(x)$ and $N_m(x)$ are the Bessel's functions of first and second kind of order m, the prime denotes the derivatives with respect to the argument x.

The effect of the fringing fields is taken into account by describing ring effective radii and effective permittivity, the former is only for microstrip ring-resonator [3—5]

$$\begin{aligned} a_{eff} &= a-\Delta W \\ b_{eff} &= b+\Delta W \\ \Delta W &= \frac{h}{\pi}\ln 2 \end{aligned} \tag{2}$$

* Assiut University Egypt

where a_{eff} and b_{eff} are the effective inner and outer radii, respectively, and h is the thickness of the substrate. The resonance frequency f_r is determined from the eigenvalue K

$$K = 2\pi f_r \sqrt{\mu\varepsilon} \tag{3}$$

μ and ε are the permeability and permittivity of the substrate material.

To give an insight into the degenerate modes "dualmode", let us consider the solution of Maxwell's equations for the electromagnetic field components [6].

$$E_Z = K^2[A_1 J_m(Kr) + B_1 N_m(Kr)] \cos m\Phi$$

$$H_r = -\frac{j\omega\varepsilon m}{r}[A_1 J_m(Kr) + B_1 N_m(Kr)] \sin m\Phi$$

$$H_\Phi = -j\omega\varepsilon[A_1 J'_m(Kr) + B_1 N'_m(Kr)] \cos m\Phi \tag{4}$$

And

$$E_z = K^2[A_2 J_m(Kr) + B_2 N_m(Kr)] \sin m\Phi$$

$$H_r = \frac{j\omega\varepsilon m}{r}[A_2 J_m(Kr) + B_2 N_m(Kr)] \cos m\Phi$$

$$H_\Phi = -j\omega\varepsilon[A_2 J'_m Kr + B_2 N'_m Kr] \sin m\Phi \tag{5}$$

The field patterns of the first resonant dual-mode "TM_{110}" are shown in Fig. 1.

Mode splitting can be performed by using nonuniform ring and symmetrically arranged coupling lines [6], [7] or by using uniform ring and asymmetrically arranged coupling lines [6].

Another version for mode splitting using asymmetrically arranged coupling lines was discussed in [8] which we will consider here.

A stripline of 50 ohm characteristic impedance is placed at a distance δ from the ring resonator edge as shown in Fig. 2a. The electric and magnetic

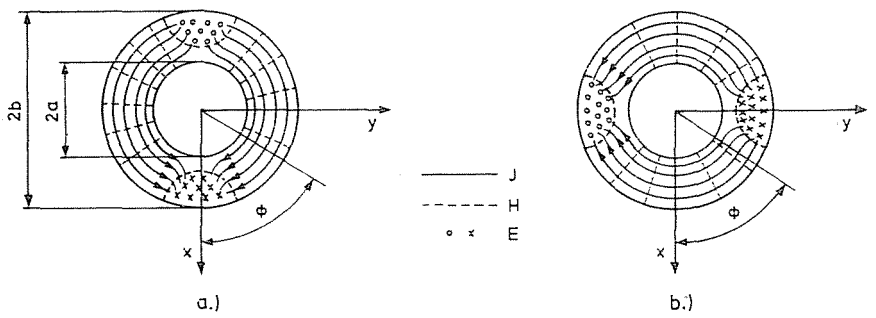

Fig. 1. Field patterns of the TM_{110} dual-mode

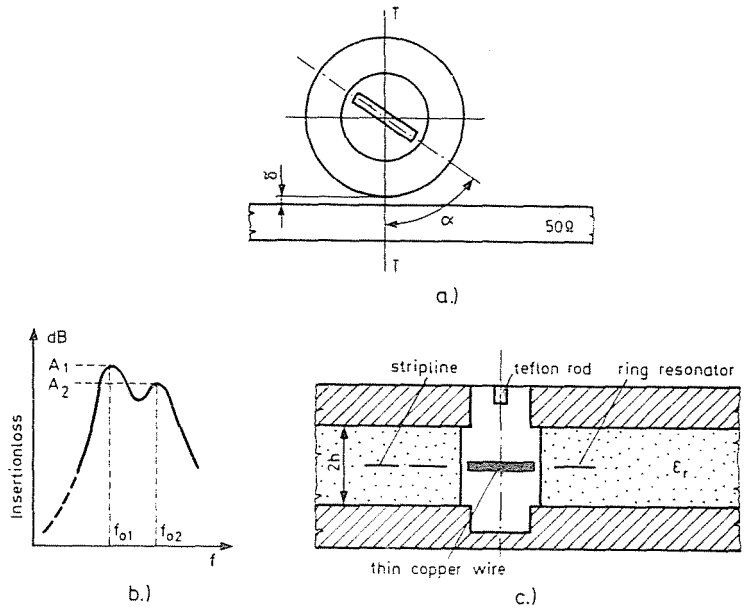

Fig. 2. "a" Ring resonator coupled with stripline asymmetrical coupling, "b" Transmission characteristic of the dual-mode ring-resonator, "c" Cross-section of the dual-mode ring-resonator with tuning element

fringing fields of the ring couple with the strip-line and dual-mode will be excited. The dual-mode ring resonator in this case possesses a band-rejection characteristic, while in [6, 7] it possesses a band-pass characteristic.

Figure 2b shows the insertion loss versus frequency of the dual-mode ring resonator shown in Fig. 1a, where f_{01} and f_{02}, A_1 and A_2 are the resonance frequencies and insertion losses at resonance of the dual-mode. Let us call the electric and the magnetic coupled modes corresponding to the field patterns of Fig. 1a and Fig. 1b, E-mode and H-mode, respectively.

Due to the difference of the coupling nature of the two modes, the presence of the strip-line perturbs the resonance frequencies of the dual mode "mode-splitting", and f_{02} is always greater than f_{01}.

The resonance frequencies of the dual-mode ring resonator can be perturbed by using tuning element in the form of a dielectric rod "Teflon rod", in which a thin copper wire is inserted so that its axis is prependicular to the dielectric rode axis, and the copper wire axis is coplanar with the ring resonator as shown in Fig. 2c. The angle α can be changed by rotating the dielectric rod, and the change of α changes the resonance frequencies. When α is zero, the two resonance frequencies are extremely splitted, f_{01} decreases, while f_{02} slightly increases. When $\alpha = \pi/2$ the two resonance frequencies are close to each other, f_{02} decreases and f_{01} slightly increases.

In other words, when α is zero $f_{01} < f_{02}$, and when α is $\pi/2$, it is possible to make $f_{02} < f_{01}$ depending on the thickness of the copper wire used in the tuning element.

Equivalent circuit of the Individual Modes

If the ring is cut at $\phi = 0$ or $\phi = \pi$, the azmithal ring current component of the H-mode will be suppressed and the H-mode completely disappears, see Fig. 1b.

Similarly, a cut in the ring at $\Phi = \pi/2$ or $\Phi = 3\pi/2$ will suppress the E-mode see Fig. 1a.

The equivalent circuits of the individual modes are shown in Fig. 3.

The normalized input admittance seen at the reference plane T – T for the E-mode shown in Fig. 3a is given by

$$Y'_{in\,1} = 1 + Y'_{r1} = 1 + \frac{1}{R'_1 + j\left(\omega L'_1 - \frac{1}{\omega C'_1}\right)} = 1 + \frac{\beta_1}{1 + jQ_{r1}\eta_{r1}} \tag{6}$$

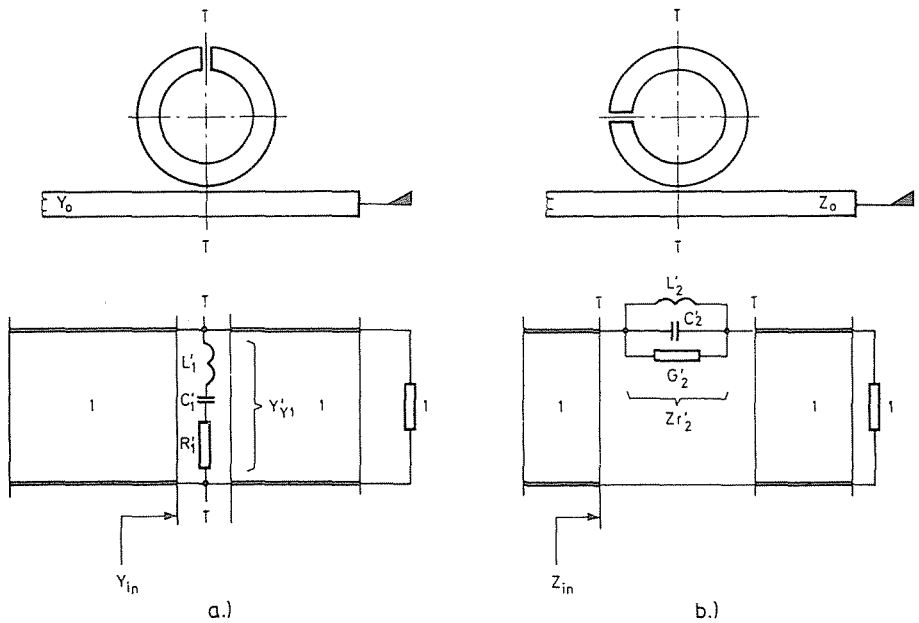

Fig. 3. Equivalent circuit of the individual modes "a" The E-coupled mode, "b" The H-coupled mode

where

$$\eta_{r1} = \frac{\omega}{\omega_{01}} - \frac{\omega_{01}}{\omega}$$

Q_{r1} is the unloaded quality factor of the E-mode and is given by

$$Q_{r1} = \frac{\omega_{01} L'_1}{R'_1}$$

β_1 is the coupling coefficient of the E-mode and is given by

$$\beta_1 = \frac{1}{R'_1}$$

The normalized input admittance can be written

$$Y'_{in\,1} = G'_{in\,1} + jB_{in\,1}$$

where

$$G'_{in\,1} = 1 + \frac{\beta_1}{1 + (Q_{r1}\eta_{r1})^2} \tag{7}$$

$$B'_{in\,1} = -\frac{\beta_1 Q_{r1\,r1}}{1 + (Q_{r1}\eta_{r1})^2} \tag{8}$$

The frequency derivatives of the normalized input conductance and normalized input susceptance are given by

$$\frac{\partial G_{in\,1}}{\partial \omega} = -\frac{2}{\omega_{01}} \beta_1 Q_{r1} \frac{Q_{r1}\eta_{r1}}{(1 + (Q_{r1}\eta_{r1})^2)^2} \left[1 + \left(\frac{\omega_{01}}{\omega}\right)^2\right] \tag{9}$$

$$\frac{\partial B_{in\,1}}{\partial \omega} = \frac{1}{\omega_{01}} \beta_1 Q_{r1} \frac{(Q_{r1}\eta_{r1})^2 - 1}{((Q_{r1}\eta_{r1})^2 + 1)^2} \left[1 + \left(\frac{\omega_{01}}{\omega}\right)^2\right] \tag{10}$$

The coefficients of the scattering matrix are given by

$$S_{11} = S_{22} = -\frac{Y'_{r1}}{2 + Y'_{r1}} = -\frac{\frac{\beta_1}{2}}{\left(1 + \frac{\beta_1}{2}\right) + jQ_{r1}\eta_{r1}} \tag{11}$$

$$S_{12} = S_{21} = \frac{2}{2 + Y'_{r1}} = -\frac{1 + jQ_{r1}\eta_{r1}}{\left(1 + \frac{\beta_1}{2}\right) + jQ_{r1}\eta_{r1}} \tag{12}$$

For the H-mode equivalent circuit shown in Fig. 3 the normalized input impedance seen at the reference plane T–T is given by

$$Z'_{in\,2} = 1 + Z'_{r2} = 1 + \frac{1}{G'_2 + j\left(\omega C_2 - \frac{1}{\omega L_2}\right)} = 1 + \frac{\beta_2}{1 + jQ_{r2}\eta_{r2}} \tag{13}$$

Where

$$\eta_{r2} = \frac{\omega}{\omega_{02}} - \frac{\omega_{02}}{\omega}$$

Q_{r2} is the unloaded quality factor of the H-mode and is given by

$$Q_{r2} = \frac{\omega_{02} C'_2}{G'_2}$$

β_2 is the coupling coefficient of the H-mode and is given by

$$\beta_2 = \frac{1}{G'_2}$$

The normalized input admittance seen at the reference plane T – T of the H-mode is given by

$$Y'_{in\,2} = \frac{1}{Z'_{in\,2}} = G'_{in\,2} + jB'_{in\,2}$$

where

$$G'_{in\,2} = \frac{1 + \beta_2 + (Q_{r2}\eta_{r2})^2}{(1 + \beta_2)^2 + (Q_{r2}\eta_{r2})^2} \tag{14}$$

$$B'_{in\,2} = \frac{\beta_2 Q_{r2}\eta_{r2}}{(1 + \beta_2)^2 + (Q_{r2}\eta_{r2})^2} \tag{15}$$

The frequency derivatives of the normalized input conductance and normalized input susceptance are given by

$$\frac{\partial G'_{in\,2}}{\partial \omega} = \frac{2}{\omega_{02}} \frac{Q_{r2}\beta_2}{(1 + \beta_2)^2} \frac{\frac{Q_{r2}\eta_{r2}}{(1 + \beta_2)}}{\left(1 + \frac{(Q_{r2}\eta_{r2})^2}{(1 + \beta_2)^2}\right)^2} \left(1 + \left(\frac{\omega_{02}}{\omega}\right)^2\right) \tag{16}$$

$$\frac{\partial B_{in\,2}}{\partial \omega} = \frac{1}{\omega_{02}} \frac{Q_{r1}\beta_2}{(1 + \beta_2)^2} \frac{1 - \left(\frac{Q_{r2}\eta_{r2}}{1 + \beta_2}\right)^2}{\left(1 + \left(\frac{Q_{r2}\eta_{r2}}{1 + \beta_2}\right)^2\right)^2} \left(1 + \left(\frac{\omega_{02}}{\omega_0}\right)^2\right) \tag{17}$$

The coefficients of the scattering matrix are given by

$$S_{11}=S_{22}=\frac{Z'_{r2}}{2+Z'_{r2}}=\frac{\dfrac{\beta_2}{2}}{\left(1+\dfrac{\beta_2}{2}\right)+jQ_{r2}\eta_{r2}} \tag{18}$$

$$S_{12}=S_{21}=\frac{Z'_{r2}}{2+Z'_{r2}}=\frac{1+jQ_{r2}\eta_{r2}}{\left(1+\dfrac{\beta_2}{2}\right)+jQ_{r2}\eta_{r2}} \tag{19}$$

The scattering matrix coefficients of the E-mode have the same form as that of the H-mode, except that there is a negative sign in S_{11}.

Thus, the insertion loss and the return loss of the two modes will have the same form.

The insertion loss is given by

$$A_i=10\log\frac{1}{|S_{21}|^2}=10\log\left(\frac{(1+\beta_i)^2+(Q_{ri}\eta_{ri})^2}{1+(Q_{ri}\eta_{ri})^2}\right) \tag{20}$$

$$R_i=10\log\frac{1}{|S_{11}|^2}=10\log\frac{\left(\dfrac{\beta_i}{2}\right)^2+(Q_{ri}\eta_{ri})^2}{\left(\dfrac{\beta_i}{2}\right)} \tag{21}$$

where $i=1, 2$ for the E-mode and H-mode, respectively. At resonance, the insertion loss is given by

$$A_i=10\log\left(1+\frac{\beta_i}{2}\right)^2 \tag{22}$$

The voltage standing wave ratio at resonance is given by

$$r_i=1+\beta_i \tag{23}$$

Thus, the coupling coefficient can be determined either from (22) or (23).

The bandwidths Δf_A and Δf_R shown in Fig. 4 are given by

$$\frac{\Delta f_{Ai}}{f_{oi}}=\frac{1}{Q_{ri}}\sqrt{1-\frac{2}{\left(1+\dfrac{\beta_i}{2}\right)^2}} \tag{24}$$

$$\frac{\Delta f_{Ri}}{f_{oi}}=\frac{1}{Q_{ri}}\left(1+\frac{\beta_i}{2}\right) \tag{25}$$

From (24) or (25) the value of Q_{ri} can be calculated.

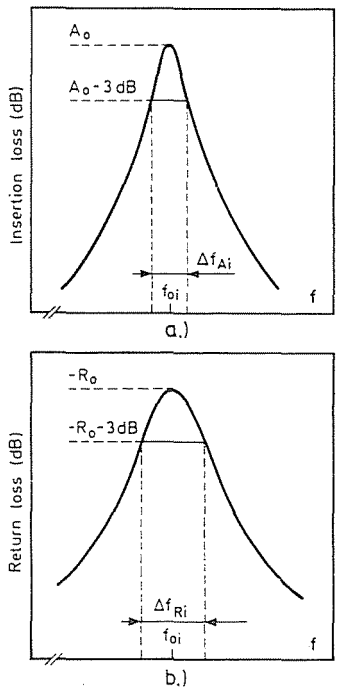

Fig. 4. The insertion and the return losses versus frequency for single mode "a" The insertion loss, "b" The return loss

The power dissipated in the ring-resonator can be calculated as follows. The incident power is given by

$$P_{in} = a_1 a_1^* = |a_1|^2$$

The reflected power is given by

$$P_{ref} = b_1 b_1^* = |S_{11}|^2 |a_1|^2$$

The transmitted power to the load is given by

$$P_{load} = b_2 b_2^* = |S_{21}|^2 |a_1|^2$$

The dissipated power in the resonator is given by

$$P_{loss} = P_{in} - P_{ref} - P_{load} = (1 - |S_{11}|^2 - |S_{21}|^2) |a_1|^2$$

The ratio of the power dissipated in the resonator to that transmitted to the load is given by

$$\frac{P_{loss}}{P_{load}} = \frac{1 - |S_{11}|^2 - |S_{21}|^2}{|S_{21}|^2} \tag{26}$$

Substituting (18) and (19) into (26), the ratio of the dissipated power in the resonator to the load power for single resonant mode is given

$$\frac{P_{loss}}{P_{load}} = \frac{\beta_i}{1+(Q_{ri}\eta_{ri})^2} \tag{27}$$

Equivalent circuit of the dual-mode

The dual-mode ring resonator shown in Fig. 2a is a symmetrical two port lossy circuit. Its equivalent circuit may be represented by a symmetrical T-section, symmetrical π-section or symmetrical lattice section.

Due to the interaction of the two modes, the lattice section, is excepted to fit for the equivalent circuit representation. Furthermore, the representation by T or π sections were found to be inadequate for the dual mode equivalent circuit. The symmetrical lattice section shown in Fig. 5a represents the equivalent circuit of the dual-mode ring resonator referred to the reference plane T – T, where

$$Z'_1 = \frac{2}{Y'_{r1}} = \frac{2}{\beta_1}(1+jQ_{r1}\eta_{r1}) \tag{28}$$

Y'_{r1} is given in (6) and

$$Z'_2 = \frac{Z'_{r2}}{2} = \frac{\beta_2}{2(1+jQ_{r2}\eta_{r2})}$$

Z'_{r2} is given in (13).

As seen from the equivalent circuit shown in Fig. 3a, when $\beta_1 = 0$ or $\beta_2 = 0$, the equivalent circuit will be reduced to one of the equivalent circuits shown in Fig. 3.

The equivalent circuit shown in Fig. 5a can be reduced to the symmetrical T-section shown in Fig. 4b [9]. Taking half section of the T-section, the eigenvalues of the scattering matrix are given by [10].

$$s_1 = \frac{Z'_1 - 1}{Z'_1 + 1}$$

$$s_2 = \frac{Z'_2 - 1}{Z'_2 + 1} \tag{29}$$

The scattering matrix coefficients are given by [10]

$$S_{12} = S_{21} = \frac{s_1 - s_2}{2} = \frac{Z'_1 - Z'_2}{(Z'_1+1)(Z'_2+1)} \tag{30}$$

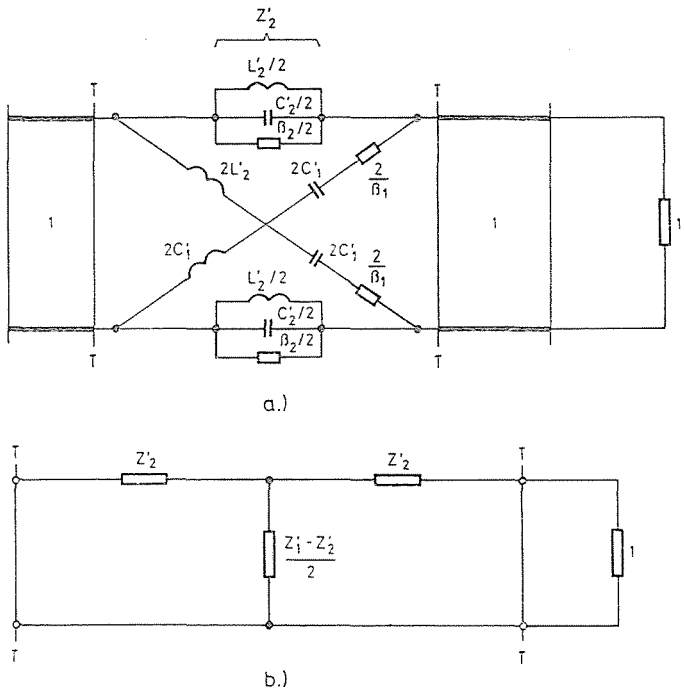

Fig. 5. Equivalent circuit of the dual-mode ring resonator "a" The lattice section equivalent circuit, "b" Its reduced T section equivalent circuit

$$S_{11}=S_{22}=\frac{s_1+s_2}{2}=\frac{Z'_1Z'_2-1}{(Z'_1+1)(Z'_2+1)} \tag{31}$$

The insertion loss A, and the return loss R of the dual-mode ring resonator are given by

$$A=10\log\frac{1}{|S_{21}|^2} \tag{32}$$

$$R=10\log\frac{1}{|S_{11}|^2}. \tag{33}$$

Substituting (28—31) into (32) and (33), one gets

$$A=10\log\frac{N_1^2+N_2^2}{D_1^2+D_2^2} \tag{34}$$

$$R=10\log\frac{N_3^2+N_4^2}{D_1^2+D_2^2} \tag{35}$$

where

$$N_1 = 1 - Q_{r1}Q_{r2}\eta_{r1}\eta_{r2} - \frac{\beta_1\beta_2}{4}$$

$$N_2 = Q_{r1}\eta_{r1} + Q_{r2}\eta_{r2}$$

$$N_3 = \frac{\beta_1 - \beta_2}{2}$$

$$N_4 = \frac{\beta_2}{2}Q_{r1}\eta_{r1} - \frac{\beta_1}{2}Q_{r2}\eta_{r2}$$

$$D_1 = 1 + \frac{\beta_1}{2} + \frac{\beta_2}{2} + \frac{\beta_1\beta_2}{4} - Q_{r1}Q_{r2}\eta_{r1}\eta_{r2}$$

$$D_2 = \left(1 + \frac{\beta_2}{2}\right)Q_{r2}\eta_{r2} + \left(1 + \frac{\beta_1}{2}\right)Q_{r2}\eta_{r2}$$

The insertion loss is infinite transmission zero, as seen from (30), and can be recognized from Fig. 5b when:

$$Z'_1 - Z'_2 = 0 \tag{36}$$

The solution of (36) implies that

$$Q_{r1}\eta_{r10} = -Q_{r2}\eta_{r20} = \pm\sqrt{\frac{\beta_1\beta_2}{4} - 1} \tag{37}$$

where η_{r10} an η_{r20} are the values of η_{r1} and η_{r2} at the frequency of transmission zero.

It is seen from (37) that the frequency of transmission zero f_{00} must lay between f_{01} and f_{02}.

The normalized input admittance at the frequency of transmission zero can be calculated referring to Fig. 5b and is given by

$$Y'_{in\,00} = \frac{2}{\beta_2}(1 + jQ_{r2}\eta_{r20}) \tag{38-a}$$

$$Y'_{in\,00} = G'_{in\,00} + jB'_{in\,00} \tag{38-b}$$

From the measured input admittance at the frequency of transmission zero, it is possible to determine the coupling coefficients using (37) and (38) and are given by

$$\beta_2 = \frac{2}{G'_{in\,00}} \tag{39-a}$$

$$\beta_1 = \frac{2}{G'_{in\,00}}|Y'_{in\,00}|^2 \tag{39-b}$$

The presence of the cuts shown in Fig. 3, suppressing one of the resonant modes affects the resonance frequency of the other mode. Furthermore, the interaction of the two modes affects also the resonance frequency of each of the two modes.

The deviations in the resonance frequencies due to mode interaction were calculated and were found to be smaller than 0.1%, and will be neglected in the following analysis.

Theoretical and experimental results

Dual mode ring resonator, with rings having fixed inner and outer radii a = 2.3 mm, b = 3.6 mm with different distances between the strip-line and the ring resonator edges $\delta = 0.1$—0.7 mm were fabricated on a 1.56 mm thickness polyguide substrate $\varepsilon_r = 2.32$.

The resonance frequency f_0 of isolated weakly coupled ring using (1), (2) and (3) was calculated and was found to be 10.88 GHz.

The transmission characteristics of these filters were measured by HP 8755 S frequency response test set. Without tuning element, the variation of the

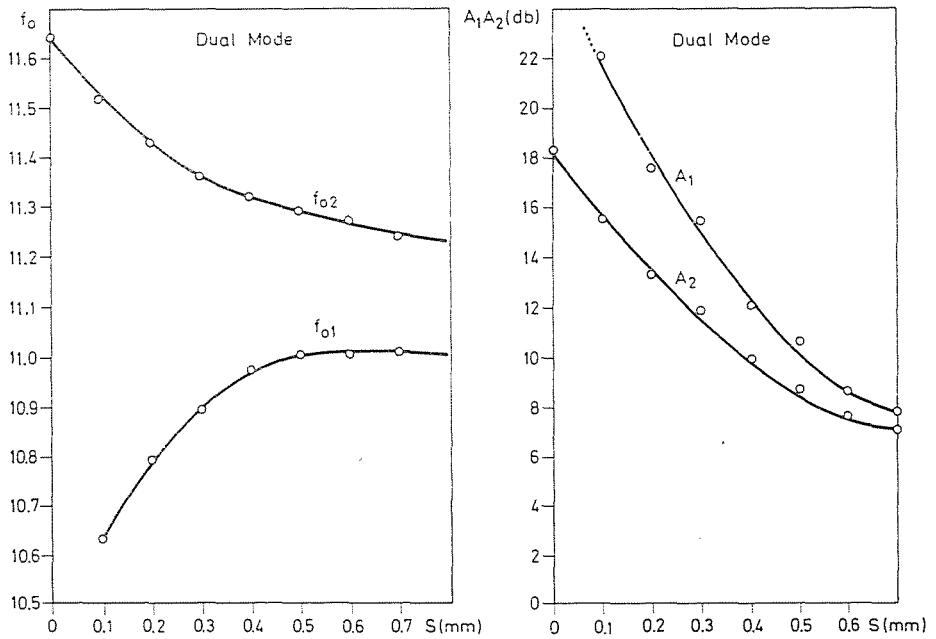

Fig. 6. "a" variation of the resonance frequencies f_{01} and f_{02} versus δ, "b" variation of the insertion losses A_1 and A_2 versus δ

resonance frequencies f_{01} and f_{02} versus δ is shown in Fig. 6a. Fig. 6b shows the variation of the insertion loss A_1 and A_2 at f_{01} and f_{02}, respectively versus δ.

The measured insertion and return loss versus frequency is shown in Fig. 7a. From (22), β_1 and β_2 were calculated, then the insertion losses were calculated using (34) and (35) and are shown in Fig. 7a for comparison. Also the variation of the susceptance slope versus frequency is shown in Fig. 7b.

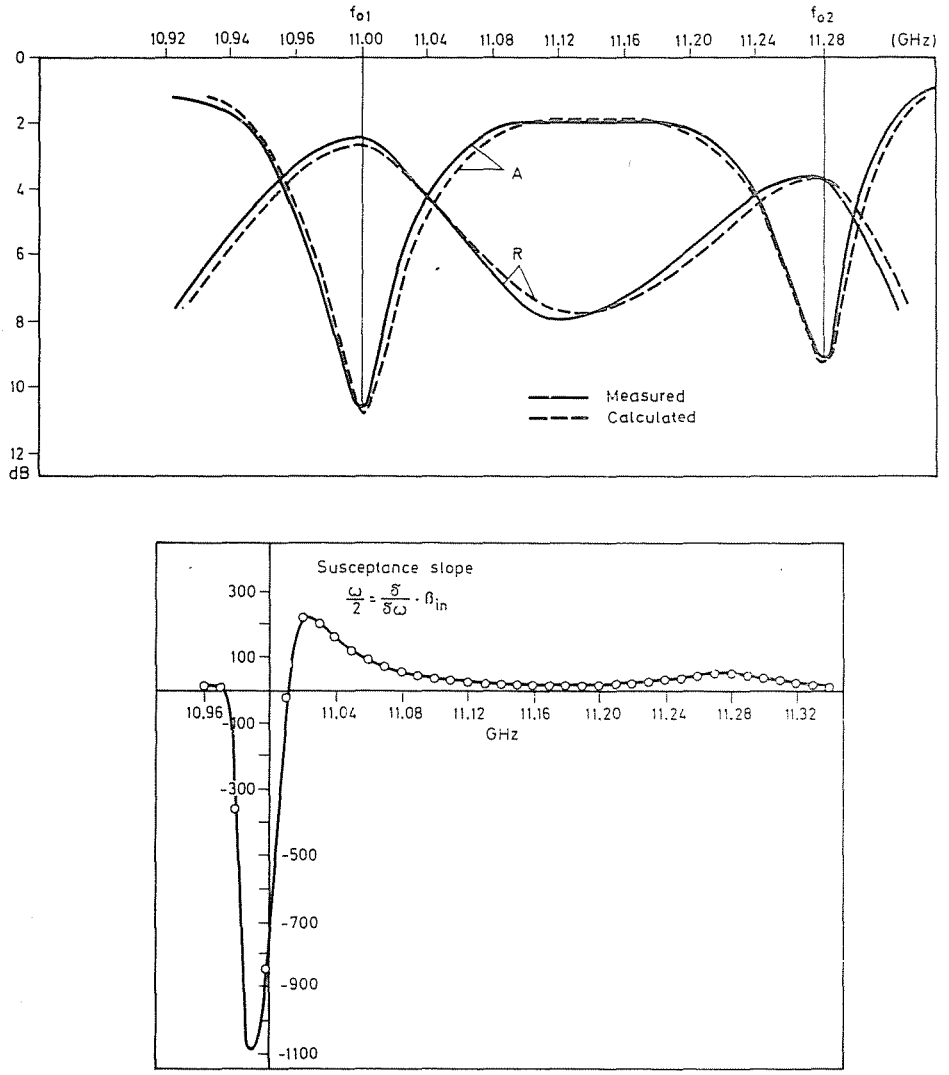

Fig. 7. "a" variation of the insertion and return losses of the dual mode ring resonator versus frequency, "b" variation of the input susceptance slope versus frequency

A tuning element was used to obtain maximum insertion loss transmission zero, where $f_{00} \cong f_{01} \cong f_{02}$. The variation of the insertion and return losses are shown in Fig. 8.

The input impedance at the frequency of transmission zero was measured and was transformed to the reference plane T—T, the effect of the SMA launcher was taken into account [11]. The calculated coupling coefficients using (39) are in good agreement with that calculated for the two individual modes equation (22).

The calculated insertion and return losses using (34) and (35) are shown in Fig. 8 for comparison.

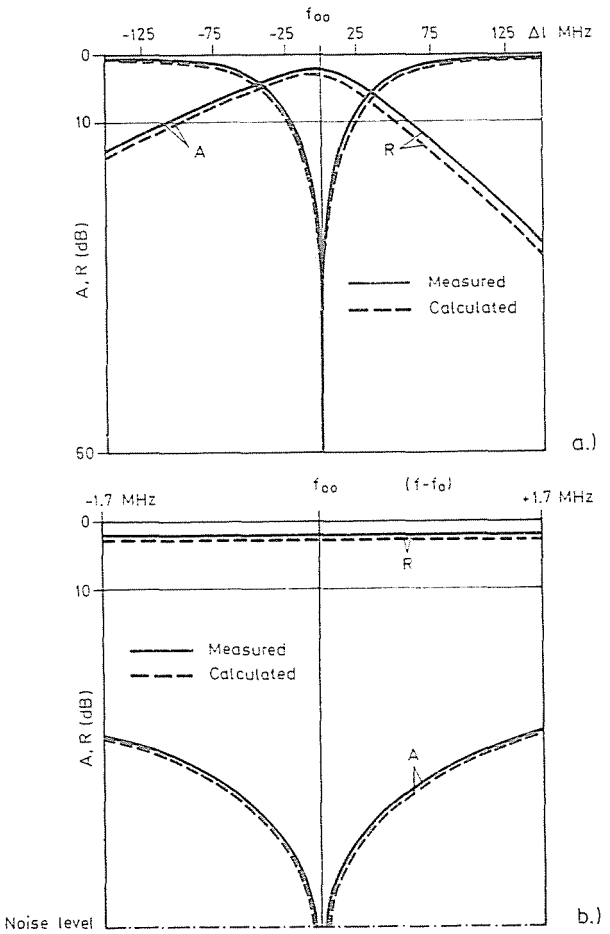

Fig. 8. Variation of the insertion and return losses of the dual-mode ring resonator tuned to show transmission zero versus frequency

For single resonant mode, the coupling coefficients can be calculated from (22) or from (23).

The two values were found to be in good agreement.

Temperature dependence of the ring-resonator

The resonance frequency of the ring resonator is obtained from the eigenvalue given in (3)

$$f_r = \frac{K_{mn}(a, b)}{2\pi\sqrt{\mu\varepsilon}}$$

$$f_r = \frac{150 K_{mn}(a, b)}{\pi\sqrt{\varepsilon_r}} \tag{40}$$

The resonance frequency of the first resonant mode is given by

$$f_r = \frac{150 K_{11}(a, b)}{\pi\sqrt{\varepsilon_r}} \tag{41}$$

The ring-resonator temperature coefficient P_r is given by

$$P_r = \frac{1}{f_r}\frac{df_r}{dT} = \frac{1}{f_r}\left(\frac{\partial f_r}{\partial \varepsilon_r}\frac{d\varepsilon_r}{dT} + \frac{\partial f_r}{\partial a}\frac{da}{dT} + \frac{\partial f_r}{\partial b}\cdot\frac{db}{dT}\right)$$

$$P_r = P_{r1} + P_{r2} \tag{42}$$

where

$$P_{r1} = \frac{1}{f_r}\frac{\partial f_r}{\partial \varepsilon_r}\frac{d\varepsilon_r}{dT} \tag{43-a}$$

$$P_{r2} = \frac{1}{f_r}\frac{\partial f_r}{\partial a}\cdot\frac{da}{dT} + \frac{1}{f_r}\frac{\partial f_r}{\partial b}\cdot\frac{db}{dT} \tag{43-b}$$

Let us begin with P_{r1} differentiating (41) with respect to ε_r and substituting in (43-a), then

$$P_{r1} = -\frac{1}{2\varepsilon_r}\frac{d\varepsilon_r}{dT} \tag{44}$$

But $\varepsilon_r(T)$ is given by [12]

$$\varepsilon_r(T) = \varepsilon_r(T_0)\,[1 + \gamma(T - T_0)] \tag{45}$$

Thus substituting (45) into (44)

$$P_{r1} = -\frac{\gamma}{2} \tag{46}$$

To determine P_{r2}, consider the characteristic equation (1)

$$F(a, b) = J_1'(K_{11}a)N_1'(K_{11}b) - N_1'(K_{11}a)J_1'(K_{11}b) \tag{47}$$

The variation in a and b cause a variation in K_{11} and consequently a variation in f_r.

Differentiating (47) with respect to

$$[J_1''(K_{11}a)N_1'(K_{11}b) - N_1''(K_{11}a)J_1'(K_{11}b)]\left(K_{11} + a\frac{\partial K_{11}}{\partial a}\right) =$$

$$= b\frac{\partial K_{11}}{\partial a}[N_1'(K_{11}a)J_1''(K_{11}b) - J_1'(K_{11}a)N_1''(K_{11}b)]$$

which can be simply written in the form:

$$\frac{1}{K_{11}}\frac{\partial K_{11}}{\partial a} = -\frac{\dfrac{\partial F}{\partial a}}{a\dfrac{\partial F}{\partial a} + b\dfrac{\partial F}{\partial b}} = \frac{1}{f_r}\frac{\partial f_r}{\partial a} \tag{48}$$

Similarly differentiating with respect to b and after simple manipulation one gets

$$\frac{1}{K_{11}}\frac{\partial K_{11}}{\partial b} = -\frac{\dfrac{\partial F}{\partial b}}{a\dfrac{\partial F}{\partial a} + b\dfrac{\partial F}{\partial b}} = \frac{1}{f_r}\frac{\partial f_r}{\partial b} \tag{49}$$

But

$$a(T) = a(T_0)[1 + \zeta(T - T_0)]$$

$$b(T) = b(T_0)[1 + \zeta(T - T_0)] \tag{50}$$

where ζ is the effective coefficient of thermal expansion of the ring resonator.

Substituting (48), (49), and (50) into (43-b) we get

$$P_{r2} = -\zeta \tag{51}$$

But ζ depends on the coefficients of thermal expansion and the modulus of elasticity of the copper and the substrate material.

If ζ_c and ζ_g are the coefficients of thermal expansions of copper and the polyguide, respectively, and E_c and E_g are the modulus of elasticity of copper and the polyguide respectively, then referring to the model shown in Fig. 9, one can get the effective coefficient of thermal expansion as follows

$$\zeta = \zeta_g \cdot \frac{1 + \frac{t}{h}\frac{E_c}{E_g}\frac{c}{g}}{1 + \frac{t}{h}\frac{E_c}{E_g}} \tag{52}$$

Substituting (46) and (51) into (42) then the value of P_r is given by

$$P_r = -\frac{\gamma}{2} - \zeta. \tag{53}$$

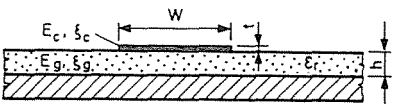

Fig. 9. Cross-section in a polyguide

From (53), the temperature dependence of the resonance frequency of the ring resonator is similar to that of the rectangular resonator. The value of P_r for the polyguide used is [12]

$$P_r = 112 \text{ ppm/°C}$$

Conclusion

The equivalent circuit of the dual mode ring resonator has been derived, its parameters were presented. The equivalent circuit interpreted the sharp attenuation characteristic of the dual mode ring resonator. The measured insertion and return losses were found to be in good agreement with the calculated values. The power dissipated in the ring resonator and the temperature dependence of the ring resonator resonance frequency were derived.

Acknowledgement

The authors wish to offer their thanks to Mr. Ferenc Völgyi for his help in adjusting and checking the measuring sets.

References

1. Vrba: Microwave planar Networks: The Annular Structure Elect. lett. *14*, 526 (1978).
2. WOLF, I.—KNOPPIK, N.: Micro-Strip-Ring-Resonator and Dispersion Measurements on Microstrip-lines Elect. Lett. *7*, 779 (1971).
3. WU, Y. S.—ROSENBAUM, F. J.: Mode chart for Microstrip-Ring-Resonator IEEE Tran. MTT. 21 pp. 487—489 July 1973.
4. Nobert—Knoppik, VDE/NTG: Vergleich und Gültigkeit verschiedener Berechnungserfahren der Resonanzfrequenzen von Mikrostrip-Ringresonatoren Nachrichtentechn. z. *29*, 141 (1976).
5. KHILLA, A. M.: Computer Aided Design for Microstrip Ring-Resonator IEEE European Microwave Conference pp. 677—681. Sep. 1981.
6. WOLF, I.: Microstrip Bandpass filter using Degenerate modes of Microstrip Ring-Resonator Elect. Lett. *8*, 302 (1972).
7. WESTED, J.—ANDERSEN, E.: Resonance splitting in nonuniform Ring Resonator Elect. Lett. *8*, 301 (1972).
8. VÖLGYI, F.—JACHIMOVITS, L.—BOZSÓKI, I.: Design of Hybrid integrated Microwave circuits on a plastic substrate Conf. on Microwave Solidstate Electronics. Gdansk (Poland) *1*, 46 (1977).
9. GÉHER, K.: Lineáris hálózatok Műszaki Könyvkiadó, Budapest, 1968. pp. 127—129.
10. ALTMAN, J. L.: Microwave Circuits D. Van Nostrand Company, Inc. 1964. chapter III.
11. CHAPMAN, A. G.—AICHISON, C. S.: A Broad-Band Model for Coaxial-to-Stripline Transition IEEE Trans. MTT-28 No. 2. pp. 130—136. Feb. 1980.

Gamal ABEDEL-RAHIEM Assiut University Egypt
dr. László JACHIMOVITS H-1521 Budapest